NACA

RESEARCH MEMORANDUM

for the

Bureau of Aeronautics, Department of the Navy

SUMMARY OF LOW-LIFT DRAG AND DIRECTIONAL STABILITY DATA FROM ROCKET MODELS OF THE DOUGLAS XF4D-1 AIRPLANE WITH AND WITHOUT EXTERNAL STORES AND ROCKET PACKETS AT MACH NUMBERS FROM 0.8 TO 1.38

TED NO. NACA DE-349

By Grady L. Mitcham, Willard S. Blanchard, Jr., and Earl C. Hastings, Jr.

Langley Aeronautical Laboratory
Langley Field, Va.

CLASSIFIED DOCUMENT

This material contains information affecting the National Defense of the United States within the meaning of the espionage laws, Title 18, U.S.C., Secs. 793 and 794, the transmission or revelation of which in any manner to an unauthorized person is prohibited by law.

NATIONAL ADVISORY COMMITTEE FOR AERONAUTICS

WASHINGTON

JUL 18 1952

NATIONAL ADVISORY COMMITTEE FOR AERONAUTICS

RESEARCH MEMORANDUM

for the

Bureau of Aeronautics, Department of the Navy

SUMMARY OF LOW-LIFT DRAG AND DIRECTIONAL STABILITY DATA FROM ROCKET MODELS OF THE DOUGLAS XF4D-1 AIRPLANE WITH AND WITHOUT EXTERNAL STORES AND ROCKET PACKETS AT MACH NUMBERS FROM 0.8 TO 1.38

TED NO. NACA DE-349

By Grady L. Mitcham, Willard S. Blanchard, Jr.,
and Earl C. Hastings, Jr.

SUMMARY

A flight investigation is being made to determine the drag and stability at low lift coefficients of $\frac{1}{10}$- scale models of the Douglas XF4D-1 airplane at Mach numbers from 0.8 to 1.38. Included herein is a summary of the low-lift drag with and without external stores and rocket packets suspended below the wing by straight unswept pylons. Some qualitative values of directional stability and pressure recovery are also included.

The drag break occurred at approximately a Mach number of 0.93 for the configurations tested. The external drag coefficient for the clean configuration was a constant value of about 0.011 at subsonic speeds and varied to about 0.038 at supersonic speeds. The addition of four rocket packets to the basic model resulted in very little increase in external drag coefficient. The addition of two external stores in combination with the four rocket packets, however, resulted in an increase in external drag coefficient of about 0.005 at subsonic speeds and 0.011 at supersonic speeds. The drag coefficient for the Douglas Aircraft Company, Inc., stores (based on maximum frontal area) which were tested independently of the model was nearly a constant value of 0.08 below the drag break which occurred at a Mach number of 0.97 and then increased abruptly to 0.22 at a Mach number of 1.15.

Some qualitative values of total-pressure recovery of the duct indicate the losses to be small throughout the Mach number range covered by the tests.

INTRODUCTION

At the request of the Bureau of Aeronautics, Department of the Navy, an investigation at transonic and low supersonic speeds of the drag and longitudinal trim characteristics of the Douglas XF4D-1 airplane is being conducted by the Langley Pilotless Aircraft Research Division. The Douglas XF4D-1 is a jet-propelled, low-aspect-ratio, swept-wing, tailless, interceptor-type airplane designed to fly at low supersonic speeds.

As a part of this investigation, flight tests were made using rocket-propelled $\frac{1}{10}$-scale models to determine the effect of the addition of external stores and rocket packets on the drag at low lift coefficients. In addition to these data, some qualitative values of the directional stability parameter C_{n_β} and duct total-pressure recovery are also presented.

SYMBOLS

M	free-stream Mach number
$\bar{c}$	mean aerodynamic chord, ft
R	Reynolds number (based on $\bar{c}$)
q	dynamic pressure, lb/sq ft
S	included wing area of model, sq ft
b	wing span of model, ft
c.g.	center-of-gravity location
$C_{D_{internal}}$	internal drag coefficient, $\frac{\text{Internal drag}}{qS}$
$C_{D_{base}}$	base drag coefficient, $\frac{\text{Base drag}}{qS}$

$C_{D_{total}}$	total drag coefficient, $\frac{\text{Total drag}}{qS}$
$C_{D_{external}}$	external drag coefficient, $C_{D_{total}} - C_{D_{internal}} - C_{D_{base}}$
C_L	lift coefficient, $\frac{\text{Lift}}{qS}$
$C_{L_{trim}}$	trim lift coefficient
C_n	yawing-moment coefficient, $\frac{\text{Yawing moment}}{qSb}$
β	angle of sideslip, deg
C_{n_β}	directional stability parameter, $\frac{\partial C_n}{\partial \beta}$
P	period of short-period lateral oscillation, sec
I_Z	moment of inertia in yaw, slug-ft^2
H/H_O	duct total-pressure recovery

MODELS AND APPARATUS

Models

Four $\frac{1}{10}$-scale models were flight-tested in this investigation. Two were of the clean configuration, one had four rocket packets added and the other was tested with four rocket packets and two Douglas Aircraft store shapes. A three-view drawing of the configurations tested is shown in figure 1 with the location and dimensions of the rocket packets and stores shown. Figures 2 to 4 are photographs of the models. The models were constructed of wood with aluminum inserts and castings. Dimensional and mass characteristics are given in table I. A fixed elevon deflection of 0.3° trailing edge up was used and the trimmer inboard of the elevons was not deflected.

In order to determine the internal drag for each model, a choking cup was designed and installed at the duct exit. This installation made it possible to obtain a Mach number of 1.0 at the exit during the

supersonic portion of the flight. An explanation of this cup installation and the method of data reduction for internal drag is given in reference 1.

The four rocket packets were suspended below the wing by straight unswept pylons. Each pylon was 2.90 inches long and the thickness ratio was 5.74 percent. Details of these pylons can be found in table II. The rocket packets were cylindrical in shape with an elliptical nose shape forward of the 23.7-percent body length and a parabolic tail section rearward of the 67.6-percent body length. The equation and ordinates of these sections are given in table II. The maximum diameter of the rocket packets was 1.03 inches and the fineness ratio was 8.4.

Two straight unswept pylons were used to suspend the external stores below the wing. Each pylon was 3.15 inches long and had a thickness ratio of 10 percent. The two external stores were finned bodies of revolution having the standard Douglas Aircraft store shape. Each had a maximum body diameter of 2.1 inches at approximately the 35-percent body length and a fineness ratio of 8.56. The body, pylon, and fin ordinates are given in table II and a revolved cross section of the pylon is given in figure 1. Two stores were also tested independently of the model. A photograph of one of the stores is shown in figure 5.

The models were boosted to approximately $M = 1.4$ by a solid fuel, 6.25-inch-diameter Deacon rocket motor which produced an average thrust of 6500 pounds for about 3.0 seconds. None of the models contained an internal rocket sustainer motor. Launching was accomplished from the zero-length launcher seen in figure 6.

Apparatus

During the flight of each model, a time history was transmitted and recorded by means of a telemeter system. Eight channels of information were measured in each model. One clean model and the model with rocket packets and external stores were instrumented to obtain normal, longitudinal, and transverse acceleration, free-stream total pressure, inlet total pressure, inlet static pressure, exit static pressure, and choking-cup base pressure. In the model with rocket packets only, the transverse accelerometer was replaced by a free-stream static-pressure pickup. In the second clean model, the duct-pressure pickups were replaced by an angle-of-attack vane and a base-pressure pickup.

Free-stream temperature and static pressure were obtained from a radiosonde released at time of firing. Ground apparatus consisted of a CW Doppler radar set and a radar tracking unit which were used to determine the model velocity and position in space.

Free-flight drag data for the stores alone were obtained by accelerating the stores to low supersonic speeds by means of a six-inch-bore compressed helium gun and tracking them with a CW Doppler radar set. Figure 7 shows a sketch of one of the model assemblies as it appeared prior to being accelerated through the gun barrel. The balsa cradles were used to aline the models in the gun barrel. Plywood push plates were used to transmit the pressure force to the assembly and to serve as a pressure seal while the assembly was in the barrel. Once free of the barrel, the cradles and push plates separated from the models.

A photograph of the compressed helium gun is shown as figure 8. After the model assembly was mounted in the breech, helium gas under a pressure of 200 pounds per square inch was allowed to expand rapidly and accelerate the model assembly through the barrel and into free flight at supersonic speed.

RESULTS AND DISCUSSION

The range of Reynolds number, based on the mean aerodynamic chord, covered by the tests is shown as a function of Mach number in figure 9. All coefficients presented, with the exception of the pylon and store drag, are based on a total wing area of 5.57 square feet. The pylon and store drag coefficients are based on the maximum cross-section area of the store. The range of trim lift coefficients for each of the tests is given in figure 10. For all data, the trim values of C_L were less than ± 0.1.

The telemeter records indicated no buffet or flutter oscillations during the flight tests.

Drag

The values for internal drag coefficient which are presented in figure 11 were obtained by the technique described in reference 1. Since only the duct inlet was geometrically similar to the full-scale airplane internally, the values of internal drag coefficient are not applicable to the full-scale airplane but were used to determine the external drag coefficient. These values of internal drag coefficient are a small percentage of external drag.

The base drag coefficient $C_{D_{base}}$ of the choking cup for each of the models is given in figure 12. This drag also represents only a very small portion of the external drag. Below $M = 0.93$, the gradual

decrease in $C_{D_{base}}$ for the model with external stores is within the accuracy of the instruments since the accuracies are somewhat reduced at subsonic speeds.

The external drag coefficients for the models are shown in figure 13. These values of external drag were obtained by the relation $C_{D_{external}} = C_{D_{total}} - C_{D_{internal}} - C_{D_{base}}$.

The duct mass-flow ratios for the models with external items and one of the clean models were a constant value of about 0.5 throughout the test speed range. This value was changed to approximately 0.6 for the second clean configuration. As can be seen in figure 13, this change in mass-flow ratio had no measurable effect on external drag.

The drag break for all the configurations occurred at a Mach number of approximately 0.93 $\left(\text{determined by assuming the drag break occurs where } \frac{dC_D}{dM} = 0.1\right)$, although the beginning of the drag rise for the model tested with two external stores in conjunction with four rocket packets was not so sharply defined as for the other tests. The small effect of external items on drag break Mach number was also indicated by the wind-tunnel transonic-bump tests reported in reference 2 and also by the results reported in reference 3 although the wing used in that investigation was of different plan form than the tests reported herein. The drag data from reference 1 have been corrected for an increment in Mach number of 0.02 on the basis of the pressure and flight-path measurements of the subsequent models tested.

The external drag coefficient for the clean configuration was nearly a constant value of 0.011 from $M = 0.8$ to $M = 0.93$, then increased abruptly to a value of 0.036 at $M = 1.0$ followed by a more gradual increase to a value of 0.038 at $M = 1.25$. Results from two tests of the clean configuration are shown plotted in figure 13. One of these models was tested primarily to obtain longitudinal-stability data. Excellent agreement, however, is shown between the external drag coefficients for the two models. Unpublished wind-tunnel results from tests of a 0.55-scale model of the clean airplane in the Ames 6- by 6-foot supersonic wind tunnel are shown plotted in figure 13 for comparison.

The addition of four rocket packets resulted in only a small increase in external drag coefficient throughout the Mach number range covered by the test. The addition of two external stores in conjunction with the four rocket packets, however, resulted in values of ΔC_D which varied from 0.005 at $M = 0.8$ to 0.008 at $M = 1.0$ and to 0.011 at $M = 1.2$;

whereas the addition of rocket packets alone resulted in a value of ΔC_D of less than 0.002 throughout the test speed range at the same Mach numbers.

Two factors possibly contributing to the high drag of this airplane are the sharp boattailing of the fuselage and the type of duct inlets used. The buckets in the drag curves at $M = 0.965$ are believed to be caused by pressure changes over the boattail which are probably the result of the formation of the shock wave on the afterbody. Tests of a parabolic body of revolution with a sharply convergent afterbody (ref. 4) indicated such changes of measured pressures over the boattail accompanied by buckets in the total drag coefficient.

Drag coefficients for the two Douglas Aircraft stores that were tested alone were identical and are presented as a function of Mach number in figure 14. These drag coefficients are based on the maximum cross-sectional area of the store and values from reference 5 are given for comparison. The drag coefficient for the store was approximately a constant value of 0.08 below the drag-break Mach number of 0.97, followed by an abrupt increase in C_D to 0.22 at $M = 1.15$. Also included in figure 14 is store-plus-pylon drag and pylon-alone drag. The pylon-drag coefficient, based on maximum cross-sectional area of the store, was estimated from the results presented in reference 6. The interference drag attributed to the store-plus-pylon installation may be obtained by subtracting the summation of the store-alone and pylon-alone drag from the increment in external drag contributed by store-plus-pylon.

Total-Pressure Recovery

Three of the models tested in this investigation had a total-pressure tube and a static-pressure orifice located in the duct at a station 9.70 inches behind the inlet. The duct is shown in detail in the three-view drawing of reference 1. Forward of this station the duct was geometrically similar to the duct in the full-scale airplane. The purpose of these pressure tubes was to determine whether twin-duct flow instability existed for the two ducts discharging into a common duct. No twin-duct instability was indicated.

The location of each total-pressure tube with respect to the duct wall is shown in figure 15 and was different for each model in order to get some indication of the profile of the total pressure across the duct at the station 9.70 inches behind the inlet. Since a thorough duct total-pressure survey was not made, the values of total-pressure recovery presented in figure 15 are qualitative but indicate only small losses in total-pressure recovery between Mach numbers of 0.80 and 1.30.

Directional Stability

As previously mentioned in the section on instrumentation, three of the models were instrumented to record lateral force. Lateral oscillations induced by disturbances at booster separation, trim change near M = 1.0, and possibly by rough air appeared on the recorded flight-time histories of these models. These oscillations have been analyzed by the single-degree-of-freedom method of reference 7.

$$C_{n_\beta} = \frac{4\pi^2 I_z}{p^2 q S b}$$

The equation given for C_{n_β} is qualified in reference 6 as applying primarily to conventional designs. Method 3 of the same reference, however, presents a solution which includes the comparatively small-order stability derivatives which are neglected in the above equation.

Values of C_{n_β} obtained by this alternate method showed very good agreement with those obtained by the given equation. This result indicated that, for this configuration, the errors in C_{n_β} due to neglecting the small-order stability derivatives were so small that the equation given previously was sufficiently accurate. Values of the rate of change of yawing moment with respect to sideslip C_{n_β} are shown in figure 16. Unpublished wind-tunnel results from tests of a 0.055-scale model of this airplane in the Ames 6- by 6-foot supersonic wind tunnel, corrected to a center-of-gravity position of 16.5 percent of the mean aerodynamic chord, have been plotted on this figure for comparison. Figure 16 shows a reduction in C_{n_β} at Mach numbers between 0.95 and 1.15. The reason for this apparent decrease is not known. Data from the model with the center-of-gravity location at $0.171\bar{c}$ indicated that the C_{n_β} values in the Mach number range between 0.85 and 0.98 were possibly erroneously high because of cross-coupling with an oscillation in pitch that is known to have occurred simultaneously with and at the same frequency as the lateral oscillation. A subsequent test, however, indicated that this apparent cross-coupling was not eliminated when the mass characteristics and center of gravity of the model were adjusted (center-of-gravity location of $0.099\bar{c}$) so that the pitch and yaw natural frequencies were not equal since the general nature of the variation of C_{n_β} with Mach number did not change. It is not known whether this condition would exist on the full-scale airplane. The maximum angle of sideslip β of the models was approximately $\pm 1^\circ$.

CONCLUSIONS

The results obtained from flight tests at low lift coefficients of $\frac{1}{10}$-scale models of the Douglas XF4D-1 airplane from a Mach number of 0.8 to a Mach number of 1.38 indicate the following conclusions:

1. The drag-break Mach number was at approximately 0.93 for all configurations. The external drag coefficient for the clean configuration was nearly a constant value of 0.011 from a Mach number of 0.8 to a Mach number of 0.93 then increased abruptly to a value of 0.036 at Mach number 1.0, followed by a more gradual increase to a value of 0.038 at Mach number 1.25. The increment in drag coefficient resulting from the addition of four rocket packets was less than 0.002 throughout the test speed range; whereas the addition of two external stores to the four rocket packets resulted in C_D increments of 0.005, 0.008, and 0.011 at Mach numbers of 0.8, 1.0, and 1.2, respectively.

2. The drag coefficient for the Douglas Aircraft Company, Inc., stores which were tested independently of the model was approximately a constant value of 0.08 below the drag break which occurred at a Mach number of 0.97 then increased abruptly to 0.22 at a Mach number of 1.15.

3. Losses in total pressure recovery between Mach numbers of 0.80 and 1.30 were small.

Langley Aeronautical Laboratory
National Advisory Committee for Aeronautics
Langley Field, Va.

Grady L. Mitcham
Aeronautical Engineer

Willard S. Blanchard, Jr.
Aeronautical Research Scientist

Earl C. Hastings, Jr.
Aeronautical Research Scientist

Approved:

Joseph A. Shortal
Chief of Pilotless Aircraft Research Division

lc

[redacted]

REFERENCES

1. Mitcham, Grady L., Blanchard, Willard S., Jr., and Hastings, Earl C., Jr.: Flight Determination of the Low-Lift Drag and Longitudinal Stability of a $\frac{1}{10}$-Scale Rocket-Powered Model of the Douglas XF4D-1 Airplane at Mach Numbers from 0.7 to 1.4. TED No. NACA DE 349. NACA RM SL51L07, Bur. Aero., 1951.

2. Anon.: Report on Wind-Tunnel Tests at Transonic Speeds of a $\frac{1}{40.2}$-Scale Left-Hand Reflection-Plane Model of the Douglas 571 Airplane. CWT Report 115, Southern Calif. Wind Tunnel, Sept 27, 1949.

3. Spreemann, Kenneth P., and Alford, William J., Jr.: Investigation of the Effects of Geometric Changes in an Underwing Pylon-Suspended External-Store Installation on the Aerodynamic Characteristics of a 45° Sweptback Wing at High Subsonic Speeds. NACA RM L50L12, 1951.

4. Stoney, William E., Jr.: Pressure Distributions at Mach Numbers From 0.6 to 1.9 Measured in Free Flight on a Parabolic Body of Revolution With Sharply Convergent Afterbody. NACA RM L51L03, 1952.

5. Muse, T. C., and Bratt, R. W.: Summary of High Speed Wind-Tunnel Tests of a Douglas Aircraft Store Shape and a 2000-Pound G.P.-AN-M66 Bomb. Rep. No. E.S. 21150. Douglas Aircraft Co., Inc., June 25, 1948.

6. Danforth, Edward C. B.: A Correlation of Experimental Zero-Lift Drag of Rectangular Wings With Symmetrical NACA 65-Series Airfoil Sections by Means of the Transonic Similarity Law for Wings of Finite Aspect Ratio. NACA RM L51G20, 1951.

7. Bishop, Robert C., and Lomax, Harvard: A Simplified Method for Determining From Flight Data the Rate of Change of Yawing-Moment Coefficient With Sideslip. NACA TN 1076, 1946.

[redacted]

TABLE I

PHYSICAL CHARACTERISTICS OF A $\frac{1}{10}$-SCALE MODEL

OF THE DOUGLAS XF4D-1 AIRPLANE

Wing:

Area (included), sq ft	5.57
Span, ft	3.35
Aspect ratio	2.01
Mean aerodynamic chord, ft	1.82
Sweepback of leading edge, deg	52.5
Dihedral (relative to mean thickness line), deg	0
Taper ratio (Tip chord/root chord)	0.33
Airfoil section at center line	NACA 0007-63/30 - 9.5° mod.
Airfoil section at tip	NACA 0004.5-63/30 - 6.6° mod.

Vertical tail:

Area (extended to center line), sq ft	0.48
Aspect ratio	2.08
Height (above fuselage center line), ft	1.00
Sweepback of leading edge, deg	66.6
Taper ratio (Tip chord/root chord)	0.26
Airfoil section at root	NACA 0008-63/30 - 9°
Airfoil section at tip	NACA 0006-63/30 - 6°45'

Elevon:

Area (one), sq ft	0.23
Span (one), ft	1.12
Chord, ft	0.22

Weight and balance:	Basic model 1 clean	Basic model 2 clean	Basic + rocket packets	Basic + packets + stores
Weight, lb	109.94	122.25	110.31	112.94
Wing loading, lb/sq ft	19.75	21.93	19.81	20.25
Center-of-gravity position, percent $\bar{c}$	16.5	9.91	16.9	17.15
Moment of inertia in yaw, slug-ft^2	4.6	5.39	4.6	

National Advisory
Committee For Aeronautics

[redacted]

TABLE 2.- STORE AND ROCKET PACKET ORDINATES

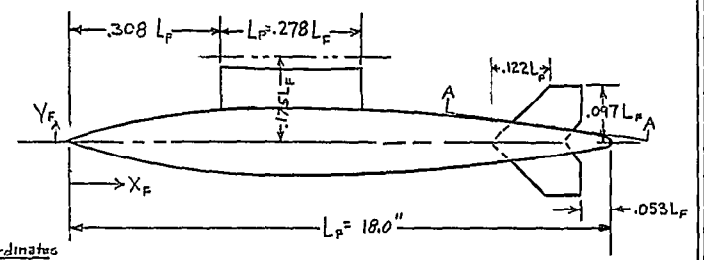

Store Ordinates

X_F/L_F	Y_F/L_F
0	0
.019	.009
.047	.020
.075	.029
.103	.035
.130	.040
.158	.044
.186	.047
.204	.050
.242	.053
.270	.055
.297	.057
.325	.0579
.353	.0583
.425	.0583
.497	.0583
.525	.0580
.553	.0575
.580	.056
.608	.055
.637	.053
.663	.051
.691	.049
.720	.046
.746	.043
.775	.040
.803	.037
.830	.0335
.858	.030
.886	.026
.914	.022
.936	.019
.958	.016
.980	.012
1.000	0
T.E. Rad. = .0055 L_F	

Section A-A

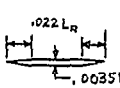

Fins have straight taper to zero thickness at tip.

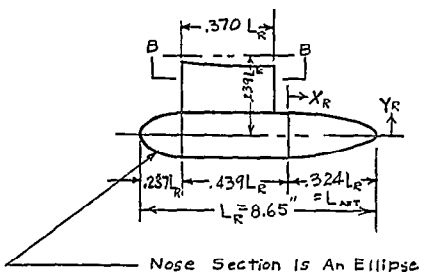

Section B-B

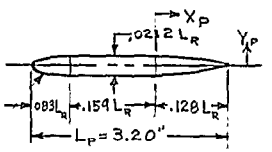

Store Pylon Ordinates

X_P/L_P	Y_P/L_P
0	0
.01	.010
.02	.014
.05	.022
.10	.031
.20	.041
.30	.047
.40	.0496
.45	.0500
.55	.0483
.65	.043
.75	.034
.85	.021
.95	.007
1.00	0
T.E. Rad. = .0035 L_P	

Rocket Packet Ordinates

X_R/L_{AFT}	Y_R/L_{AFT}
0	.1841
.0715	.1835
.143	.1805
.214	.177
.286	.171
.357	.165
.428	.157
.500	.148
.572	.137
.643	.125
.713	.109
.785	.091
.858	.071
.928	.048
.965	.033
.983	.024
1.000	0

Rocket Packet Pylon Ordinates

$X_R/L_{P_{AFT}}$	$Y_R/L_{P_{AFT}}$
0	.0824
.147	.0797
.286	.0728
.428	.0627
.572	.0504
.715	.0360
.858	.0199
.929	.0111
1.000	0

NACA

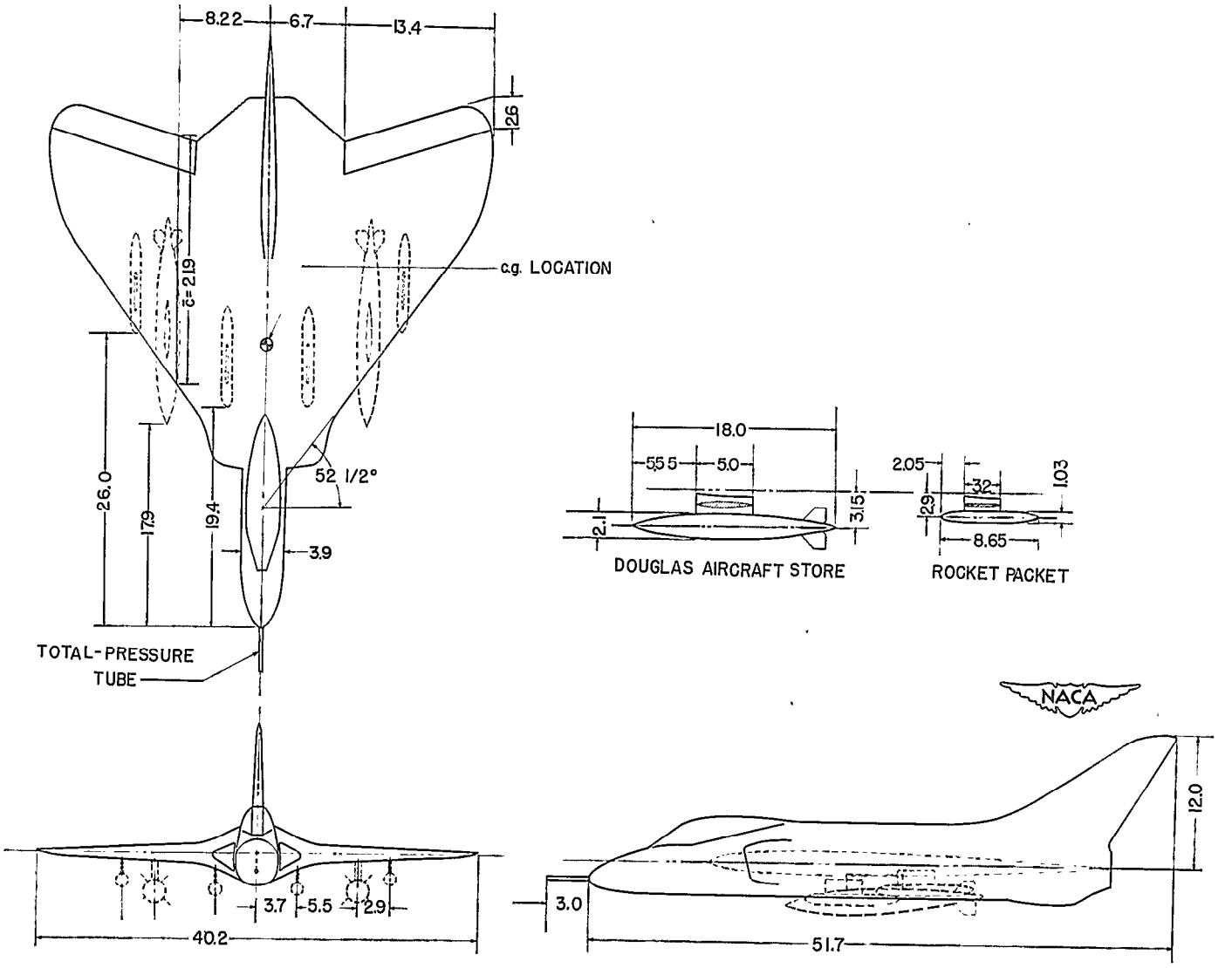

Figure 1.- Three-view drawing of the model. All dimensions are in inches.

NACA
L-71138

Figure 2.- Photograph of the clean configuration.

Figure 3.- Photograph of the model with four rocket packets.

Figure 4.- Photograph of the model with four rocket packets and two fuel stores.

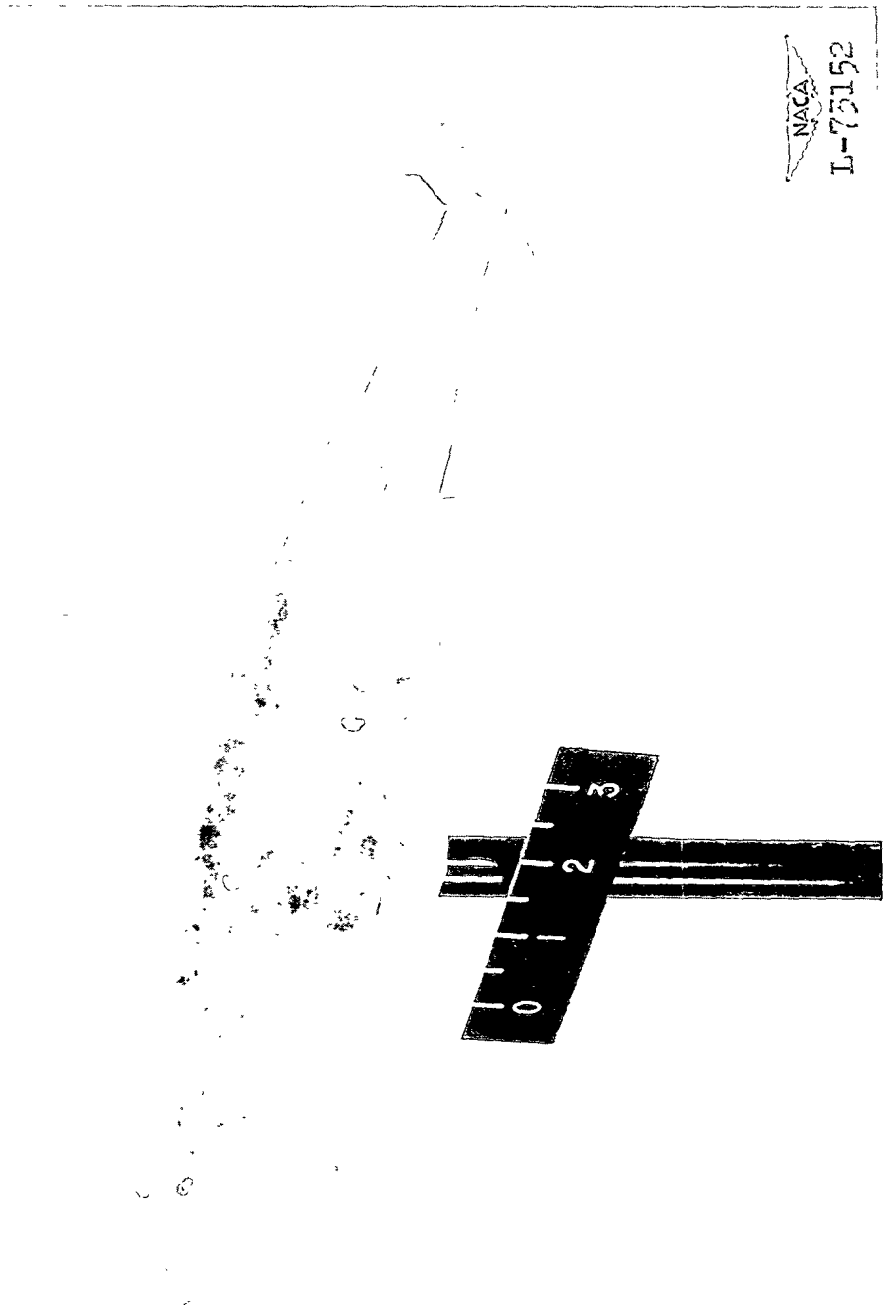

Figure 5.- Photograph of the Douglas Aircraft Company store.

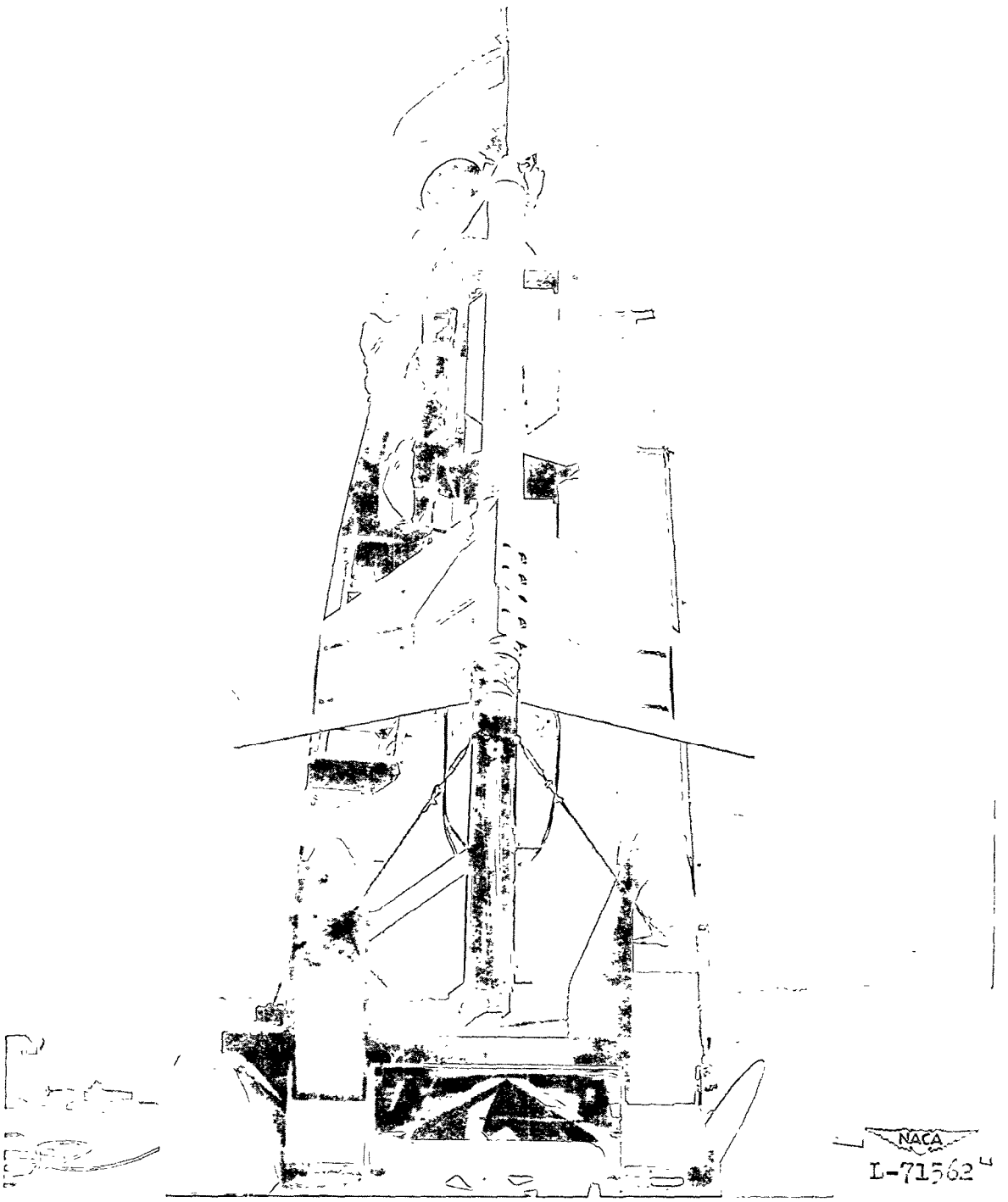

Figure 6.- Photograph of one of the booster-model combinations on the launcher.

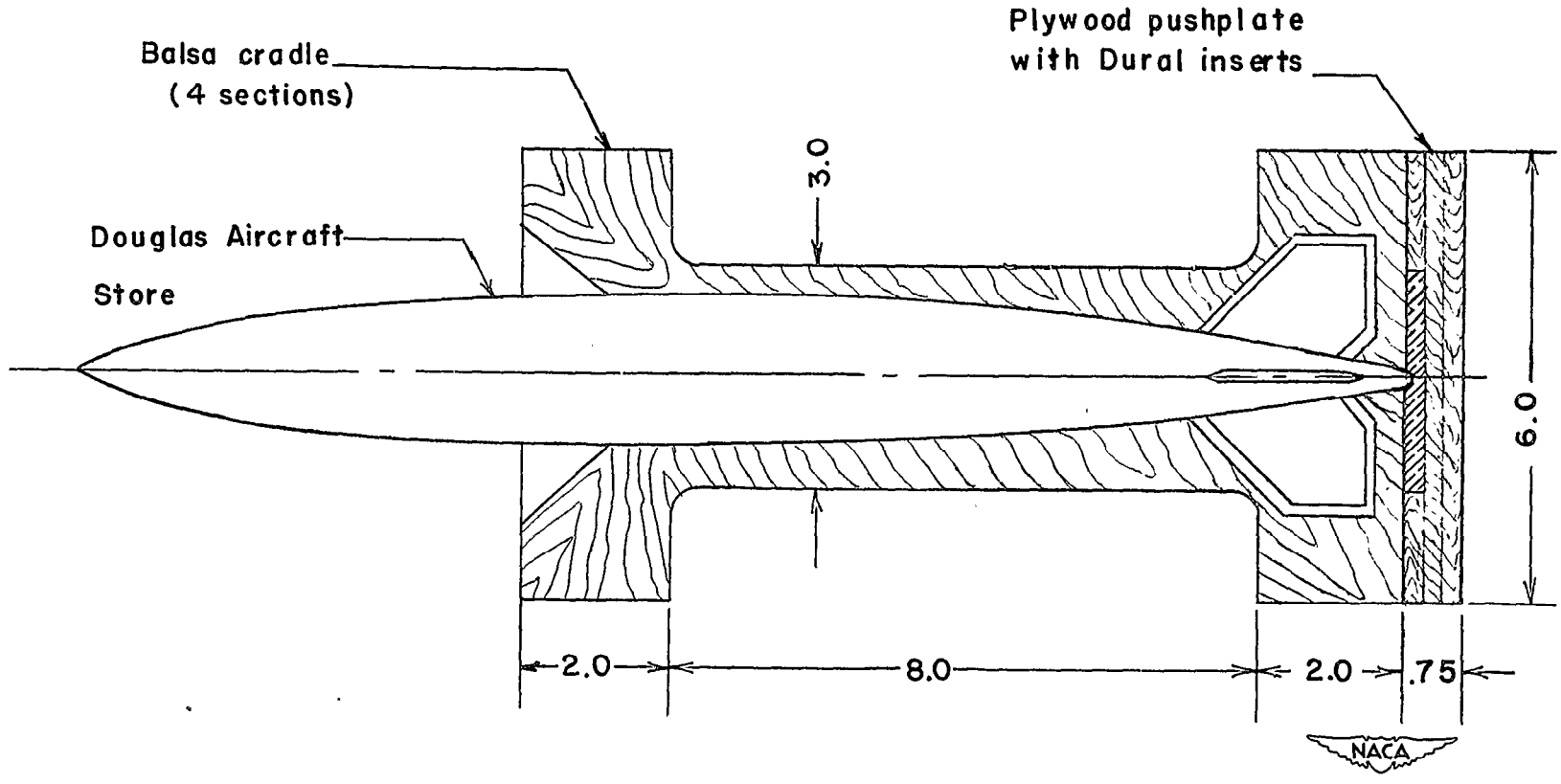

Figure 7.- Douglas Aircraft store test assembly. All dimensions are in inches.

Figure 8.- Photograph of the compressed helium gun.

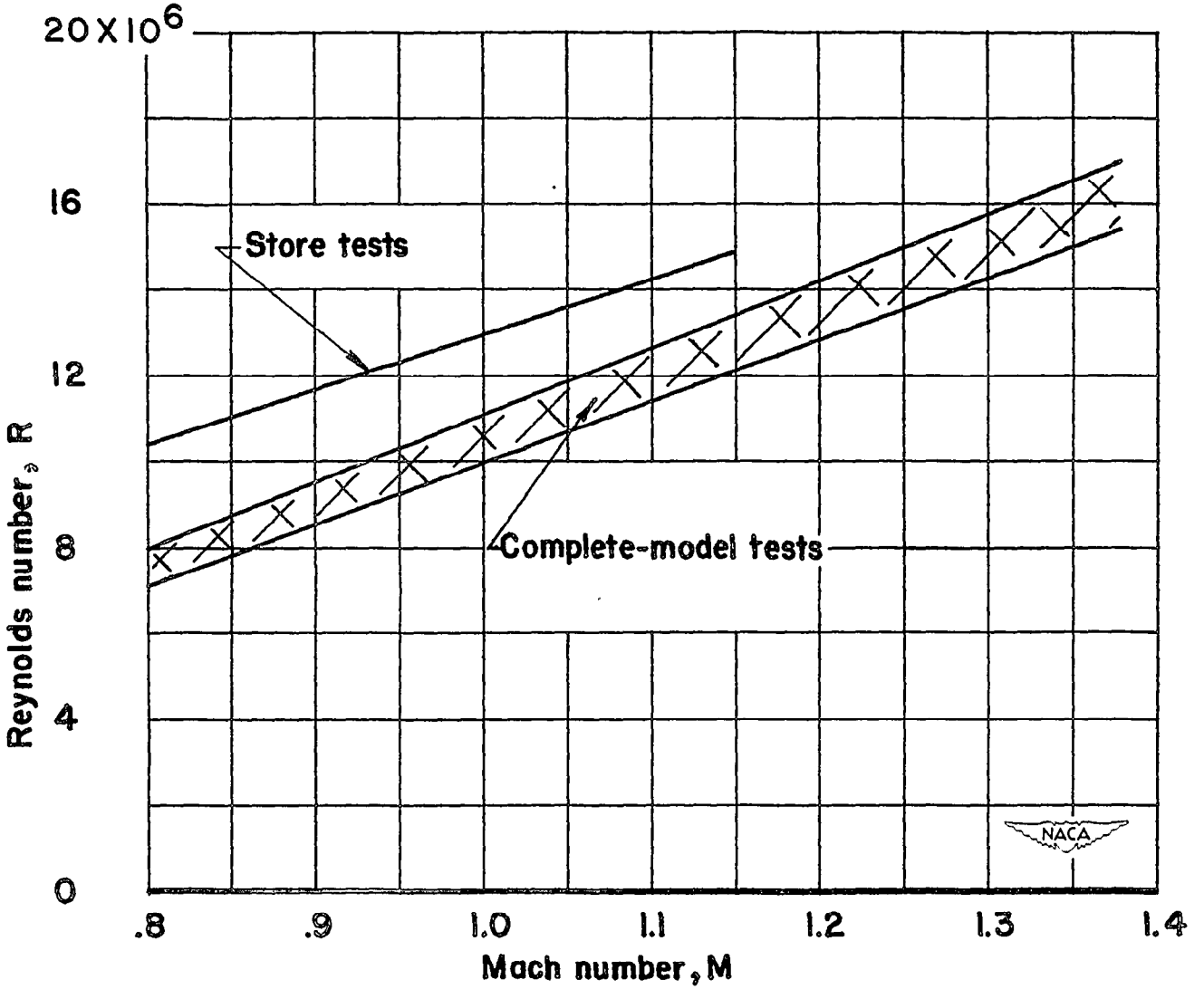

Figure 9.- Variation of Reynolds number with Mach number.

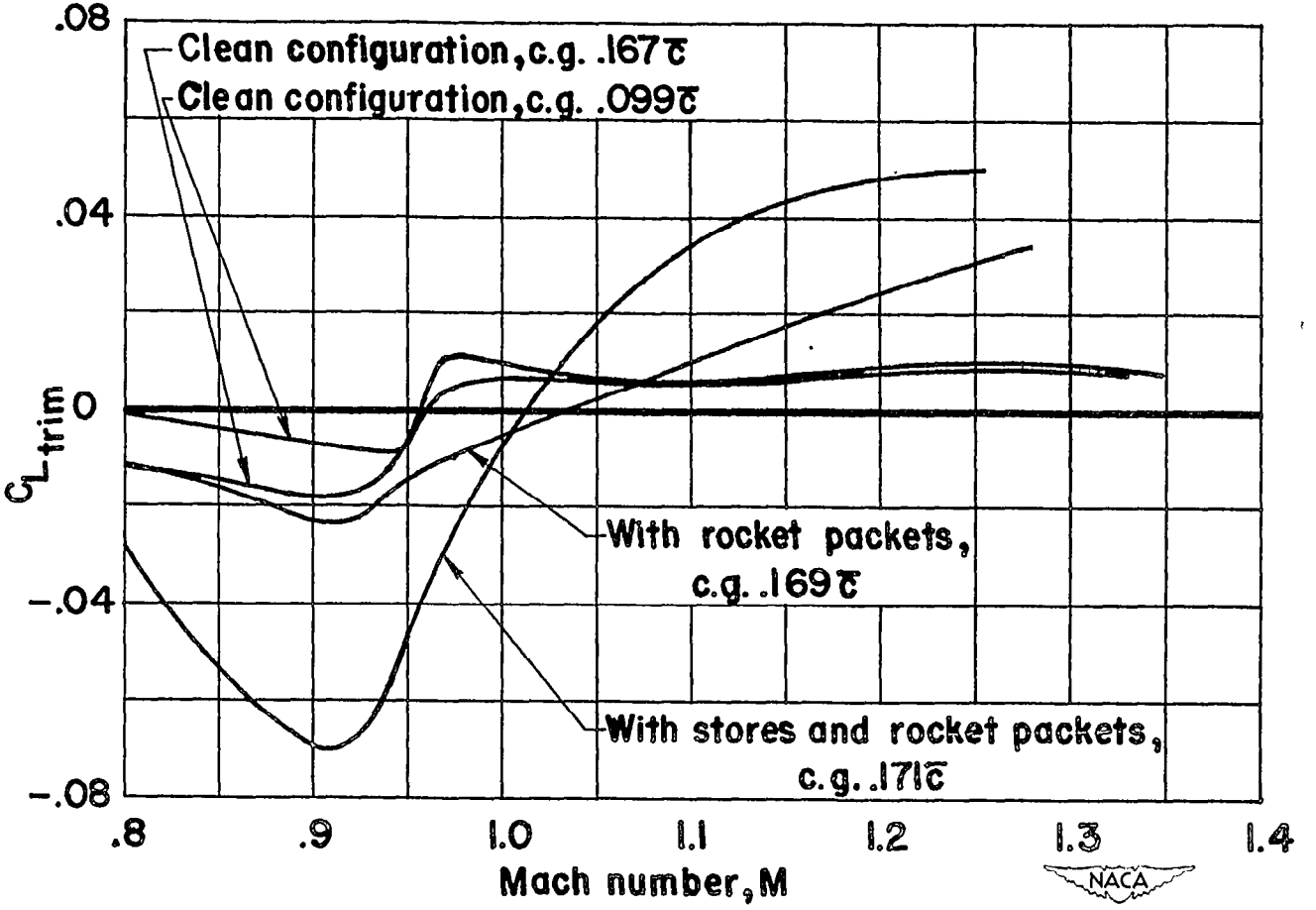

Figure 10.- Trim-lift coefficient.

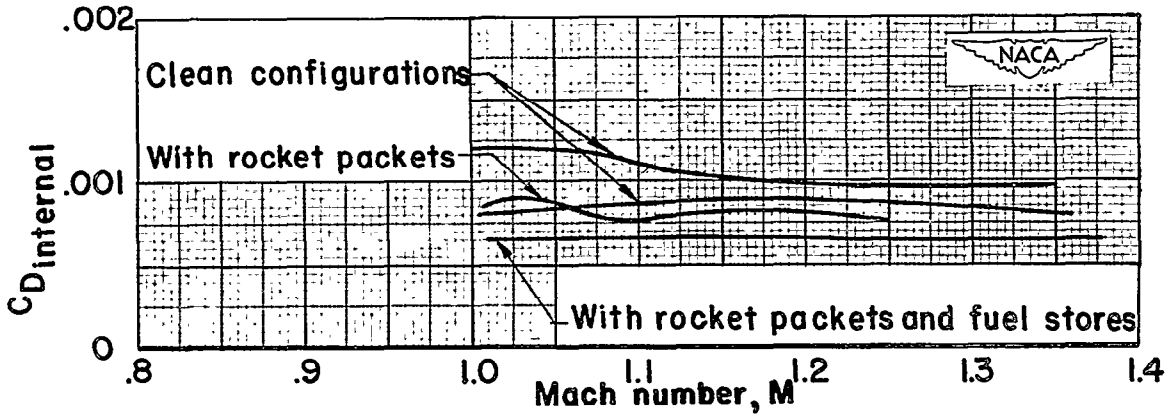

Figure 11.- Internal-drag coefficient.

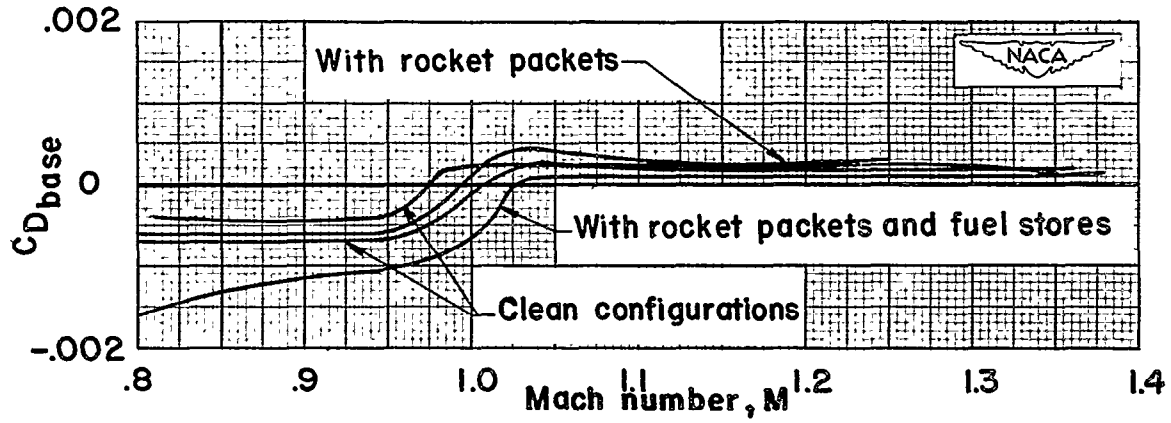

Figure 12.- Base-drag coefficient.

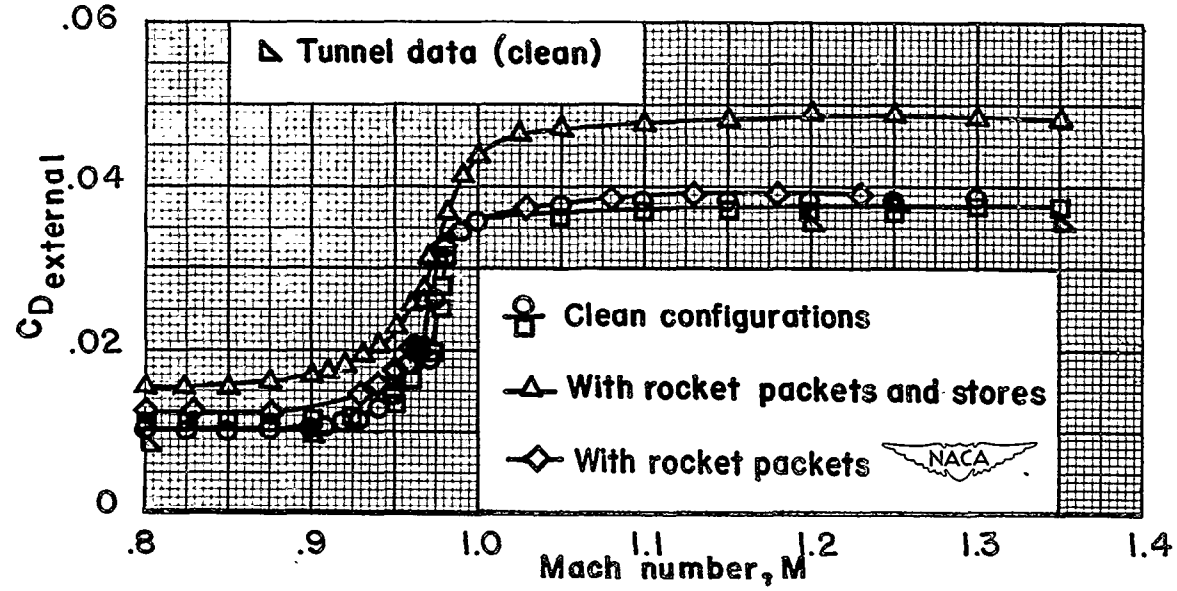

Figure 13.- External-drag coefficient.

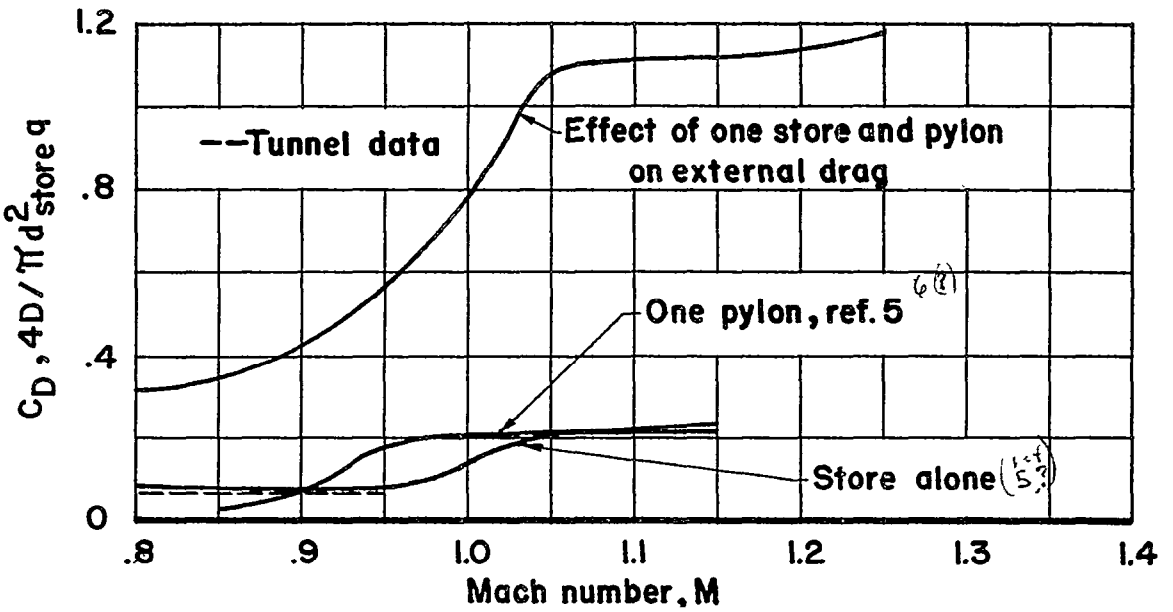

Figure 14.- Store, pylon, and store-plus-pylon drag.

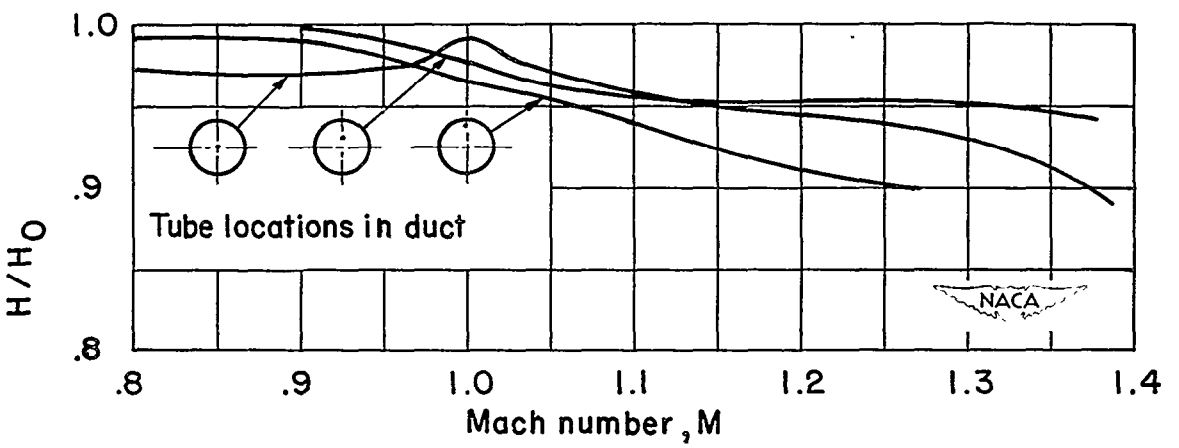

Figure 15.- Total-pressure recovery indicated by the tube located 9.70 inches behind the duct inlet.

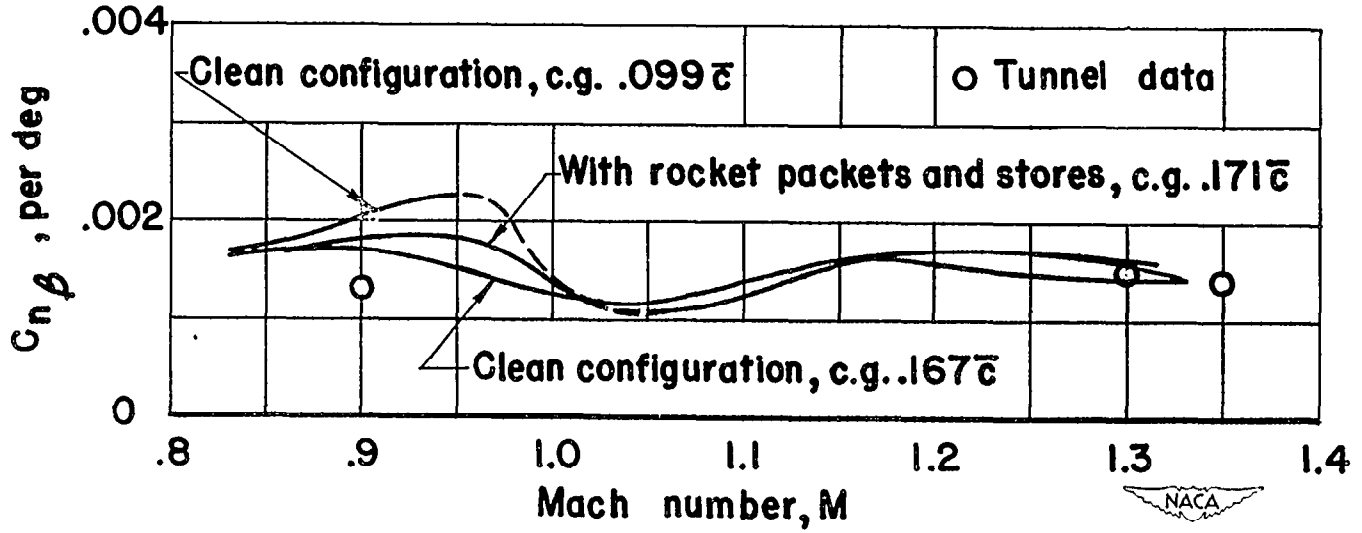

Figure 16.- Variation with Mach number of the rate-of-change of yawing-moment coefficient with respect to angle of sideslip.